This article has been accepted for inclusion in a future issue of this journal. Content is final as presented, with the exception of pagination.

Extending Electrostatic Modeling for Schottky p-GaN Gate HEMTs: Uniform and Engineered p-GaN Doping

Mojtaba Alaei, Matteo Borga, Elena Fabris, Stefaan Decoutere, Johan Lauwaert, and Benoit Bakeroot

***Abstract*— This article presents a comprehensive analytical framework for modeling p-GaN gate high-electron-mobility transistors (HEMTs) based on rigorous solution of the Poisson and Schrödinger equations. It focuses primarily on the calculation of the 2-D electron gas (2DEG), voltage variation across the junction (ΔV_j), and AlGaN barrier (ΔV_b) for the entire range of forward gate bias until gate breakdown. Our model considers the impact of AlGaN barrier height saturation. In addition, we demonstrate our model with the engineered p-GaN doping profile that yields higher forward gate breakdown voltages. Gate capacitance and breakdown voltage have been modeled for both uniform and engineered p-GaN doping profiles. The viability and accuracy of the proposed model are demonstrated through comparisons with empirical measurement data and TCAD simulations.**

***Index Terms*— Barrier voltage, breakdown, forward bias gate leakage current, junction voltage, p-GaN doping engineering, p-GaN gate HEMTs, uniform p-GaN doping.**

I. Introduction

GALLIUM nitride-based high-electron-mobility transistors (HEMTs) demonstrate outstanding performance in high-frequency and high-power applications due to the superior properties of wide-bandgap GaN material, such as high electron mobility, high density of 2-D electron gas (2DEG), and high critical electric field [1], [2]. However, a notable drawback is their default "normally-ON" state. Introducing a p-GaN cap layer between the AlGaN layer and gate metal is widely acknowledged as an effective approach to achieve a positive threshold voltage [3]. In spite of the existence of established compact models, such as the Advance SPICE model [4], the EPFL HEMT model [5], [6], and the MIT Virtual Source GaN HEMT-High Voltage (MVSG-HV) model [7], which have demonstrated maturity in capturing the characteristics of normally-ON GaN HEMTs, the modeling of various physical aspects associated with Schottky p-GaN gate HEMTs remains in an immature state and requires further attention. The focus of this study is on the investigation of Schottky contacted p-GaN devices rather than ohmic contacted p-GaN devices, given that the former represents the prevalent choice among manufacturers in the current landscape. The presence of two back-to-back diodes in p-GaN gate HEMTs poses challenges for accurate modeling of critical phenomena. Given the rapid progress in manufacturing processes and device technologies, the development of precise, physically based compact models is essential to facilitate the design and optimization of wide-bandgap (integrated) circuits. In order to investigate critical parameters, such as breakdown voltage and forward bias gate leakage current, it is imperative to model the voltage distribution between the two back-to-back diodes (Schottky and p-i-n diodes). Several simplified models have been developed to describe parameters, such as the variation in voltage across the Schottky junction (ΔV_j) and the AlGaN barrier layer (ΔV_b). Among these models, some use an iterative approach, equating the leakage current equations of Schottky diode and p-i-n diode to extract ΔV_j and ΔV_b [8]. Others rely on a simplified two-series capacitor model [9]. Notably, two distinguished models are proficient in analytically describing ΔV_j and ΔV_b. One method involves analyzing the Mg doping within the p-GaN layer and solving the 1-D Poisson equation, which requires complex mathematical calculations to model ΔV_j and ΔV_b [10]. The other approach utilizes charge equality between dual-series capacitance, offering a more compact representation of these variables [11]. However, these models primarily exhibit validity for medium-voltage levels, overlooking crucial factors, such as AlGaN barrier height saturation. Consequently, they fail to account for phenomena, such as 2DEG charge saturation at high gate-to-source voltage (V_{GS}) levels [12]. It is our objective in this article to develop a compact model that allows to determine the voltage drops for ΔV_j and

Manuscript received 25 July 2024; accepted 16 August 2024. This work was supported by European Union's Horizon 2020 Research and Innovation Program through the ASCENT+ Project under Grant 871130. The review of this article was arranged by Editor K. Alam.
(Corresponding author: Mojtaba Alaei.)

Mojtaba Alaei and Benoit Bakeroot are with the Center for Microsystems Technology (CMST) and the Interuniversity Microelectronics Centre (IMEC), Ghent University, 9052 Ghent, Belgium (e-mail: Mojtaba.Alaei@ugent.be; Benoit.Bakeroot@ugent.be).

Matteo Borga, Elena Fabris, and Stefaan Decoutere are with the Interuniversity Microelectronics Center (IMEC), 3001 Leuven, Belgium.

Johan Lauwaert is with the Liquid Crystals and Photonics Group (LCP), Ghent University, 9052 Ghent, Belgium.

Color versions of one or more figures in this article are available at https://doi.org/10.1109/TED.2024.3446488.

Digital Object Identifier 10.1109/TED.2024.3446488

© 2024 The Authors. This work is licensed under a Creative Commons Attribution 4.0 License. For more information, see https://creativecommons.org/licenses/by/4.0/

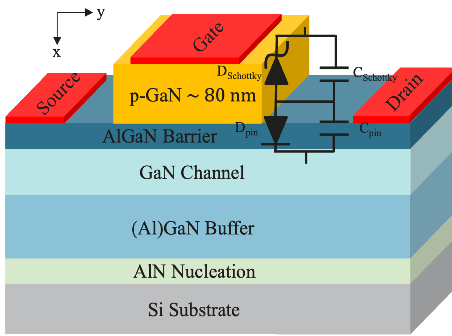

Fig. 1. Three-dimensional schematic view of a Schottky p-GaN gate HEMT with uniform p-GaN doping.

ΔV_b for forward gate bias voltages V_{GS} up till breakdown. In this article, we used a model that incorporates the 2DEG charge density through a self-consistent approach involving the simultaneous solution of Poisson and Schrödinger equations. Furthermore, the saturation of the AlGaN barrier band bending is considered, which results in charge transfer from the 2DEG into and over the AlGaN barrier, and recombination with holes in the 2-D hole gas (2DHG) at the interface between the p-GaN and AlGaN layers. In this article, the structure is as follows. In Section II, we describe the p-GaN gate HEMT structure and investigate the energy band diagram. In Section III, a charge-based model is used to model ΔV_j and ΔV_b over a range of low voltages up to breakdown, taking into account charge saturation within the 2DEG. In Section IV, we elaborate on doping profile engineering, which results in enhancements in p-GaN gate HEMTs. We utilize our model to provide insights into the mechanisms driving these improvements through our results and develop a framework for gate capacitance and breakdown voltage prediction. Through validation via technology computer-aided design (TCAD) simulations and experimental data, our model demonstrates a high degree of agreement with empirical measurements.

II. Structure and Physical Analysis

In Fig. 1, a prototype cross section of a p-GaN gate HEMT featuring a Schottky gate is depicted. The p-GaN layer, utilized exclusively in the gate section of the device, exhibits electrically active uniform doping, with a Mg chemical doping level denoted as N_A. A comprehensive analysis of this structure to gain a thorough understanding of the underlying physics governing breakdown voltage and gate leakage conduction is needed. Our initial step in device analysis involves the examination of the band diagram under equilibrium conditions, as illustrated in Fig. 2. Based on the information presented in the band diagram and under the condition of a small V_{GS}, we can draw the following conclusions:

$$V_{\mathrm{GS}} = \varphi_{bn} + V_{bi} + \Delta V_j + \psi_{s1} + \frac{\Delta E_{c1} - \Delta E_{c2}}{q} - V_{b0} + \Delta V_b - \psi_{\mathrm{ch0}} + \Delta \psi_{\mathrm{ch}} \quad (1)$$

where φ_{bn} represents the Schottky barrier height of the metal toward the conduction band; V_{bi} is built-in voltage; ΔV_j is the variation of the junction voltage drop at a given V_{GS};

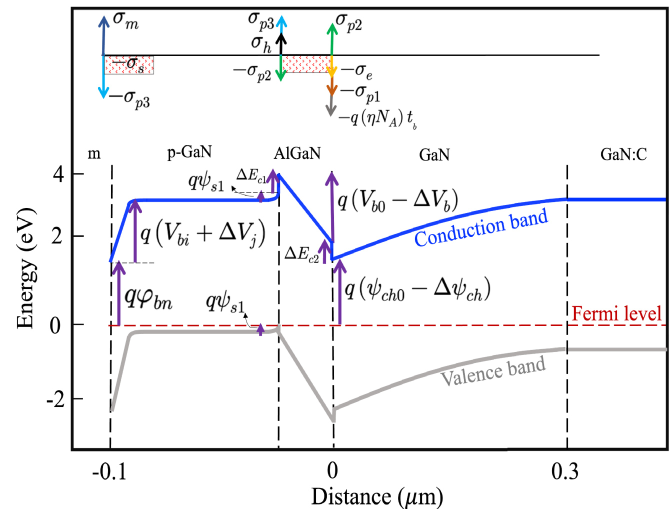

Fig. 2. Energy band diagram of p-GaN gate HEMT at equilibrium condition ($V_{\mathrm{GS}} = 0\,V$).

ψ_{s1} representing the surface potential at the p-GaN/AlGaN interface; ΔE_{c1} and ΔE_{c2} denoting voltage discontinuities between the p-GaN layer and the barrier, and between the barrier and the GaN channel, respectively, are considered equal ($\Delta E_{c1} = \Delta E_{c2}$); V_{b0} is defined as the AlGaN barrier voltage drop under equilibrium conditions ($V_{\mathrm{GS}} = 0V$); ΔV_b is the variation of the AlGaN voltage drop at a given V_{GS}; ψ_{ch0} is the energy gap between the conduction band and the Fermi level at the channel interface under equilibrium conditions; and $\Delta\psi_{\mathrm{ch}}$ is variation of the energy gap at the given V_{GS}. V_{bi} is determined by the equation $V_{bi} = (E_g/q) + (\chi/q) - (k_B T/q)\ln((N_V/p_1)) - \phi_m$, with χ and ϕ_m representing GaN's electron affinity and the metal's work function, respectively; N_V is effective valence band density of states (Dos); k_B is Boltzmann's constant; and $p1$ is hole density obtained from [13]. The quantity denoted as ψ_{ch0} can be derived from the band diagram information at the equilibrium condition and can be expressed as follows:

$$\psi_{\mathrm{ch0}} = \varphi_{bn} + V_{bi} + \psi_{s1} + \frac{\Delta E_{c1} - \Delta E_{c2}}{q} - V_{b0}. \quad (2)$$

Substituting (2) into (1) yields

$$V_{\mathrm{GS}} = \Delta V_j + \Delta V_b + \Delta\psi_{\mathrm{ch}}. \quad (3)$$

Equation (3) substantiates the distribution of the gate voltage across the Schottky junction voltage, AlGaN barrier, and energy gap, respectively. In the next section, a detailed explanation of the modeling for ΔV_j, ΔV_b, and $\Delta\psi_{\mathrm{ch}}$ across a range of V_{GS} voltages, from low to high, is presented.

III. Extending Charge-Based Model of Voltage Distribution Among ΔV_j, ΔV_b, and $\Delta\psi_{\mathrm{CH}}$

Fig. 1 also depicts the dual-series capacitance framework described in [11]. Table I lists the physical parameters of p-GaN gate HEMTs. Considering the principle of charge equality in both capacitors and channel, ($\delta Q_{\mathrm{ch}} = \delta Q_{\mathrm{Schottky}} = \delta Q_{\text{p-i-n}}$), we proceed to establish the charge-based expressions for ΔV_b and ΔV_j. By placing a Gaussian box around the

This article has been accepted for inclusion in a future issue of this journal. Content is final as presented, with the exception of pagination.

TABLE I
PHYSICAL PARAMETERS OF P-GAN/ALGAN/GAN HEMT USED IN THE MODEL DERIVATIONS

Parameter	Symbol	Value
Al Mole Fraction	x	0.215
GaN permittivity	ε_{GaN}	8.9
AlGaN permittivity	ε_b	$8.9 - 0.4x$ [5]
GaN band gap	E_g	3.4 eV
AlGaN Thickness	t_b	14 nm
Bandgap Difference Between AlGaN and GaN	ΔE_g	$(6.2-3.4)\,x-0.8\,[x\,(1-x)]$ eV [16]
Conduction band discontinuity between AlGaN and GaN	ΔE_{c2}	$0.68\Delta E_g$ eV [17]
Effective conduction band density of states	N_C	$\sim\ 3\times10^{18}$ cm^{-3} [18]
Effective valence band density of states	N_V	$\sim\ 2.5\times10^{19}$ cm^{-3} [5]
Mg chemical doping level of p-GaN layer	N_A	$\sim\ 2.25\times10^{19}$ cm^{-3}
Non-ideality factor	m	0.6
Electron affinity	χ	4.1 eV
Experimentally determined parameter	γ_0	$2.12\times10^{-12}\ Vm^{4/3}$ [5], [19]

AlGaN/GaN-channel interface [14], this yields the charge neutrality equation $\sigma_h+\sigma_{p3}-\sigma_{p2}+\sigma_{p2}-q(\eta N_A)t_b-\sigma_e-\sigma_{p1}=0$, and considering the equality between the polarization charges in the p-GaN and GaN layers ($\sigma_{p3}=\sigma_{p1}$), and the fact that σ_{p2}, representing polarization charges per unit area of the barrier, cancels out within the equation, and considering the negligible impact of channel charge ($\sigma_e = qn_{2\mathrm{DEG}}$) at the equilibrium state ($\sigma_e \approx 0$), the negative depleted charge of $q(\eta N_A)t_b$ will be balanced by the sheet charge density localized precisely at the interface between the AlGaN barrier and the p-GaN (σ_h), given by $\sigma_h = q(\eta N_A)t_b$.

The parameter η denotes the proportion of p-GaN doping that diffuses into the barrier. The range of variation for the parameter η typically spans from 0.1 to 0.2, as evidenced by documented sources and observed measurements [10], [15].

As the gate-to-source voltage V_{GS} increases, the 2DEG density ($n_{2\mathrm{DEG}}$) can no longer be disregarded, and in order to maintain charge neutrality, this additional $\sigma_e = qn_{2\mathrm{DEG}}$ will be balanced by an additional hole charge denoted as σ_h^* at the p-GaN/AlGaN interface ($\sigma_h+\sigma_h^*$), where $\sigma_h^* = qn_{2\mathrm{DEG}}$. In other words, the AlGaN barrier height will decrease as follows:

$$V_{b0}-\Delta V_b = \frac{\sigma_{\mathrm{pol}}-(\sigma_h+qn_{2\mathrm{DEG}})}{C_b}. \quad (4)$$

Here, $V_{b0} = (\sigma_{\mathrm{pol}}-\sigma_h/C_b)$ denotes the voltage drop across the AlGaN barrier under equilibrium conditions ($V_{\mathrm{GS}} = 0V$) and similarly, $\Delta V_b = (qn_{2\mathrm{DEG}}/C_b)$ represents the variation of the voltage drop across the AlGaN barrier for a given V_{GS}.

The polarization charge density at the AlGaN/GaN interface is $\sigma_{\mathrm{pol}} = \sigma_{p2}-\sigma_{p1}$ (see inset of Fig. 2), and C_b corresponds to the capacitance associated with the AlGaN barrier and is defined as $C_b = (\varepsilon_b/t_b)$. Equation (4) is crucial as it predicts saturation in the 2DEG density at a specific gate bias in a p-GaN gate HEMT. This saturation prevents the AlGaN barrier voltage from attaining a negative value. At a specific gate voltage, the 2DEG charge peaks, ensuring that electron and hole emissions over the barrier begin before the barrier voltage reaches 0 V, affirming the practical significance of the model's predictions.

In the given context, the net polarization charge at the $Al_xGa_{1-x}N$/GaN (where x is the Al mole fraction) interface can be estimated from [10] $\sigma_{\mathrm{pol}} = 0.104x-0.0282x(1-x)$. Hence, based on the preceding analysis and employing a charge-based model as described in [11], the expressions for ΔV_j and ΔV_b are as follows:

$$\Delta V_b = \frac{qn_{2\mathrm{DEG}}}{C_b} \quad (5)$$

$$\Delta V_j = V_{bi}\left(\sqrt[\frac{1}{1-m}]{1+(qn_{2\mathrm{DEG}})\times\sqrt{\frac{2(1-m)^2}{qN_A\varepsilon_{\mathrm{GaN}}V_{bi}}}}-1\right). \quad (6)$$

The parameter m represents a dimensionless nonideality factor ranging between 0 and 1. Through a thorough analysis of the self-consistent solution to the coupled Poisson's and Schrödinger's equations, following the methodology outlined in [20], the parameter $\Delta\psi_{\mathrm{ch}}$, which equals the variation of the Fermi energy level ($\Delta\psi_{\mathrm{ch}} = E_f/q + V_{\mathrm{TH}}$, where V_{th} is the threshold voltage), has been meticulously determined and subsequently expressed in the form of a cubic polynomial representation. Increasing V_{GS} raises $\Delta\psi_{\mathrm{ch}}$, leading to a decrease in the total gap at the channel interface ($\psi_{\mathrm{ch0}}-\Delta\psi_{\mathrm{ch}}$). This representation allows for an analytical expression of the Fermi energy level in relation to the applied gate-to-source voltage V_{GS}. Detailed explanations of this equation can be found in the given reference. In Fig. 3, $\Delta\psi_{\mathrm{ch}}$ is plotted against V_{GS}. A strong agreement is observed between the model (blue solid line) and TCAD simulation results (red circles). The subsequent analysis takes into account other relevant aspects while acknowledging the importance of the equation previously mentioned. Weak accumulation 2DEG charge is derived by combining the subthreshold and moderate regions, where, notably, the 2DEG charge demonstrates a linear dependency on the Fermi energy specifically in the moderate region, as described by Deng et al. [20]

$$n_{\mathrm{Total}} = \mathrm{Dos}\,V_{\mathrm{th}}\exp\left(-\frac{|E_f|}{qV_{\mathrm{th}}}\right)+K_3E_f/q. \quad (7)$$

In this context, the modeling incorporates the Dos, the thermal voltage (V_{th}), and the Fermi energy level (E_f), derived from the self-consistent solution of the Poisson–Schrödinger equations.

The function K_3 facilitates the transition from the moderate region to the strong inversion region. This function can be determined by setting the 2DEG charge in the moderate

This article has been accepted for inclusion in a future issue of this journal. Content is final as presented, with the exception of pagination.

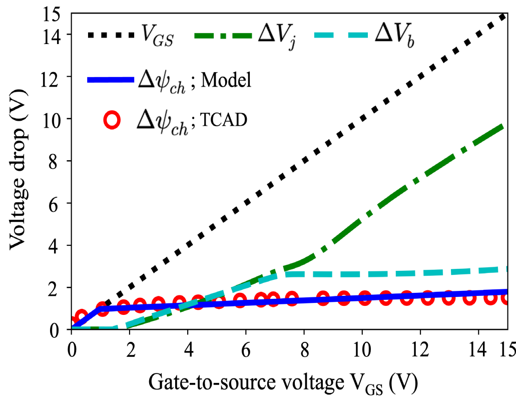

Fig. 3. Variation of $\Delta\psi_{ch}$ (model and TCAD simulation), ΔV_j, and ΔV_b as a function V_{GS}.

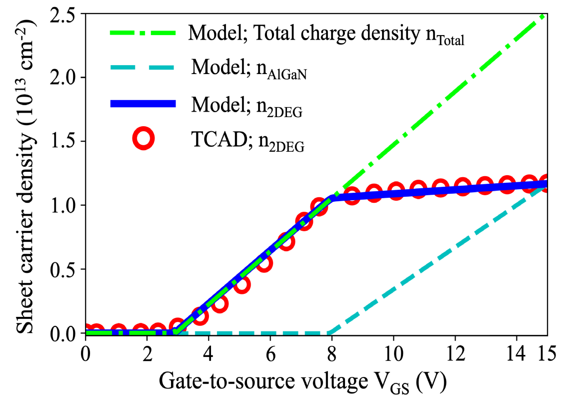

Fig. 4. Comparison of 2DEG charge density model (solid line) with TCAD simulation results (circle), alongside total channel charge density and AlGaN barrier charge density.

region ($K_3 E_f/q$) equal to the simplified Schrödinger equation in the strong inversion region ($\mathrm{Dos}(E_f/q - \gamma_0 n_{s0}^{2/3})$) at the condition $E_f = E_0$, where $n_{s0} = \mathrm{Dos} V_{\mathrm{th}} ln2$. The expression for K_3, denoted by $K_3 = f\mathrm{Dos}/(1 + \mathrm{Dos}\gamma_0 n_{s0}^{-1/3})$, signifies its dependence on different parameters.

The smoothing function $f = 1/[1 + \exp(-\zeta(V_{\mathrm{GS}} - V_{\mathrm{TH}}))]$ facilitates a transition between the weak inversion and moderate regions, and the symbol ζ represents a fitting parameter.

The expression representing the 2DEG charge (n_{Total}) under strong accumulation conditions using the Poisson equation is as follows [20]:

$$n_{\mathrm{Total}} = \frac{C_d}{q}\left(V_{G0} - E_f/q\right). \tag{8}$$

C_d represents the capacitance per unit area between the gate electrode and 2DEG, which can be extracted to achieve improved matching, and $V_{G0} = V_{\mathrm{GS}} - V_{\mathrm{TH}}$. By combining (7) and (8), the total charge density (n_{Total}) will be extracted. The proposed model governing the n_{Total} remains applicable as long as the Fermi energy (E_f) remains below the threshold of ΔE_{c2}. Beyond this threshold, the AlGaN barrier experiences the maximum reduction in height, leading to a saturation of AlGaN band bending. As a result of this saturated band bending, electrons can be emitted from the 2DEG into and over the AlGaN barrier and recombine with holes in the 2DHG to maintain the charge balance between the 2DHG and the 2DEG ($\delta n_{\mathrm{2DEG}} = \delta n_{\mathrm{2DHG}}$) [14]. In order to model n_{2DEG}, that is valid for the entire V_{GS} range, the emitted electrons from the channel (referred to as n_{AlGaN}) should be subtracted from n_{Total}. In Fig. 4 (marked by red circles), the simulated TCAD data reveal the charge density beneath the gate electrode. This visualization illustrates the saturation of the 2DEG charge, occurring at an approximate voltage of 8 V. Nevertheless, the saturation of the 2DEG charge is not complete, as there is a slight increase observed. This phenomenon is attributed to the nonconstant nature of the Fermi energy (E_f) above the threshold region. By employing the commonly used estimation method of the Fermi–Dirac integral in degenerate semiconductors referenced in [21], integrating across the AlGaN layer, and further simplifying for valid $E_f > \Delta E_{c2}$, the resulting expression for the AlGaN charge can be found in [19]

$$n_{\mathrm{AlGaN}} = \frac{\varepsilon_b N_C\left(E_f - \Delta E_{c2} + k_B T\ ln(c)\right)}{qc\left(\sigma_{\mathrm{pol}} - qn_{\mathrm{2DEG}}\right)}. \tag{9}$$

The parameter c is a numerical constant used to simplify Fermi–Dirac statistics, as shown in [22]. To further model the distribution of electron charge within the AlGaN layer, Swamy and Dutta [22] introduced a distinctive slope control factor $(1 - \beta V_{G0}/V_{\mathrm{GSAT}})$, where V_{GSAT} denotes the voltage level at which the n_{2DEG} approaches the σ_{pol} value, aiming to improve accuracy, notably under higher gate biases. We employ the subsequent analytical equation [22]. Equation (10), shown at the bottom of the next page.

In the given equation set, where A represents C_d/q, $B = A/(\mathrm{qDos})$, and β denotes a fitting parameter. The function Z is defined, such that, for all values of E_f where $E_f < \Delta E_{c2} - k_B T\ ln(c)$, Z is equal to 0, and for all values of E_f where $E_f > \Delta E_{c2} - k_B T\ ln(c)$, Z becomes $(E_f - \Delta E_{c2} + k_B T\ ln(c))/q$.

The expression for variable Z is defined as follows:

$$Z = 0.5 \times \left(\alpha + \sqrt{\alpha^2 + (0.25\delta)^2} - 0.25\delta\right) \tag{11}$$

where δ is a smoothing parameter, $\alpha = (E_f - \Delta E_{c2} + k_B T\ ln(c))/q$, and T is the temperature. Fig. 4 presents a comparative analysis between the proposed model and the TCAD simulation results, demonstrating a commendable level of agreement. In accordance with the behavior of the 2-D electron gas (2DEG), the voltage drop across the barrier will also reach saturation [see (5)], thereby allocating the remaining voltage drop across the upper Schottky diode (i.e., the junction voltage). The distribution of junction voltage, barrier voltage, and energy gap is illustrated graphically in Fig. 3.

As depicted in Fig. 3, when $V_{\mathrm{GS}} < V_{\mathrm{TH}}$, the entire gate voltage drops across the energy gap $\Delta\psi_{\mathrm{ch}}$. Conversely, for $V_{\mathrm{GS}} > V_{\mathrm{TH}}$, $\Delta\psi_{\mathrm{ch}}$ approaches saturation, causing an increase in ΔV_b and ΔV_j based on the previously presented charge-based equations (5) and (6). When the Fermi energy exceeds $\Delta E_{c2} - k_B T\ ln(c)$ and the AlGaN barrier height reaches its maximum reduction, ΔV_b becomes saturated, and the remaining gate voltage drops across ΔV_j. Research efforts

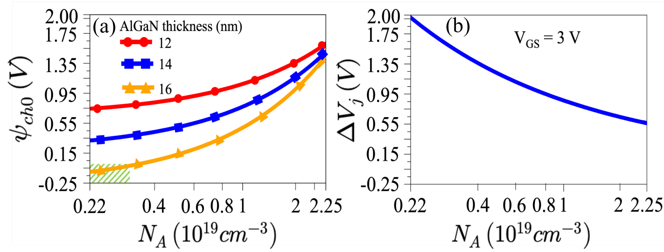

Fig. 5. (a) Variation of ψ_{ch0} and (b) ΔV_j as the functions of the logarithmic scale of N_A (p-GaN doping concentration). The green highlight indicates normally ON operation, particularly evident at $t_b = 16$ nm.

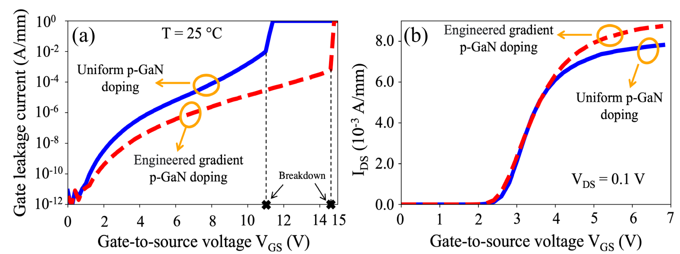

Fig. 6. Measurement of (a) gate leakage current and (b) drain-to-source current for both the uniform p-GaN doping device and the engineered gradient p-GaN doping device.

have previously focused primarily on scenarios involving low gate voltages when modeling ΔV_j and ΔV_b drops. This study extends the investigation to include the impact of charge saturation, inducing a saturation phenomenon in the behavior of the barrier voltage. We have modeled ΔV_j and ΔV_b drops for the entire range of gate forward bias voltages until breakdown.

IV. Doping Profile Engineering

Equation (6) inherently establishes a direct correlation between the junction voltage and the p-GaN doping level (N_A). Fig. 5(a) and (b) illustrates the dependence of ψ_{ch0} and ΔV_j on the logarithmic scale of p-GaN doping. As depicted in Fig. 5(a), reducing the doping concentration across the p-GaN layer impacts the η term, leading to an augmentation of V_{b0} [see (4)] and a reduction in the threshold voltage. Fig. 5(a) clearly shows that, under the given doping conditions, AlGaN with 12- and 14-nm layer thicknesses maintains a positive zero-bias energy gap (ψ_{ch0}), indicating a device with normally-OFF behavior. However, for an AlGaN barrier with a 16-nm layer thickness, the zero-bias energy gap (ψ_{ch0}) falls below zero within the green highlighted region ($\sim N_A < 0.3 \times 10^{19}$ cm^{-3}). This shift signifies that the device is no longer in a normally-OFF state. Note that the impact of the N_A on ψ_{ch0} (and thus V_{TH}) is mainly through η [see (4)], and that this will depend on the exact growth conditions in reality. An effective approach to reduce the forward bias gate leakage current and to increase the gate forward breakdown voltage is by lowering the p-GaN doping. This reduction results in a higher depletion depth and subsequently increases ΔV_j [Fig. 5(b)]. However, this reduction in doping density presents a challenge in terms of maintaining a relatively high value for the threshold voltage. IMEC has successfully implemented an innovative technique involving a gradient p-GaN doping method [23]. This implementation includes the incorporation of a low-doped p-GaN cap layer above a high-doped p-GaN layer, offering a favorable solution. Specifically, the process involves growing a 30-nm p-GaN layer counter-doped with Si ($\sim 0.75 \times 10^{19}$ cm^{-3}), resulting in a net p-type active doping of around $\sim 5 \times 10^{18}$ cm^{-3} on top of a 60-nm p-GaN layer (electrically active doping: 2.25×10^{19} cm^{-3}) according to the findings in [23]. This technique increases the depletion depth and junction voltage drop, thereby mitigating the electric field and increasing the breakdown voltage without impacting the η term. Fig. 6(a) and (b) depicts the measurement of gate leakage current and drain current with respect to forward bias V_{GS} for both the uniform p-GaN doping device and the engineered gradient p-GaN doping device. A notable reduction in forward bias gate leakage current and an increase in breakdown voltage are observed, while the threshold voltage remains unchanged [Fig. 6(b)]. It is important to note that in Fig. 6(a), the 1-A/mm plateau corresponds to the compliance limit of the source measure unit (SMU), reached after the catastrophic failure of the gate of the device. A detailed analysis and modeling of the gate leakage current and I–V characteristics for uniform and engineered doping profile are presented in our previous work [24]. For a comprehensive understanding, we direct the reader to that reference.

In the next sections, we will elucidate the impact of the doping profile engineering on the characteristics of capacitance–voltage (C–V) behavior, breakdown outcomes, and proceed to construct a corresponding model.

A. Impact of Doping Profile Engineering on Gate Capacitance: Model and Verification

Here, we present an analysis of gate capacitance model in p-GaN gate/AlGaN/GaN heterostructures employing a dual-junction capacitor model. The model is founded upon the concept of two-series capacitances, visually depicted in Fig. 1. This model, despite its simplicity, proves to be a valuable tool for device designers in obtaining reasonably accurate capacitance estimations. In this model, the Schottky capacitance (C_{Schottky}) and p-i-n capacitance ($C_{\text{p-i-n}}$) are configured in series, leading to the expression of equivalent gate capacitances as follows:

$$\frac{1}{C_G} = \frac{1}{C_{\text{p-i-n}}} + \frac{1}{C_{\text{Schottky}}}. \quad (12)$$

The capacitance of the p-i-n diode can be determined through the simplified equation ($C_{\text{p-i-n}} = (qn_{\text{2DEG}}/\Delta V_b +$

$$n_{\text{AlGaN}} = \frac{\varepsilon_b N_C\left(1 - A\beta\left(qV_{G0}/\sigma_{\text{pol}}\right)\right) \times (Z)}{c \times \left[\sigma_{\text{pol}} - \left[\text{qAV}_{G0}/(1+B)\right] \times \left(1 - A^{2/3}\gamma_0/\left[(1+B)^{2/3}V_{G0}^{1/3}\right]\right)\right]}. \quad (10)$$

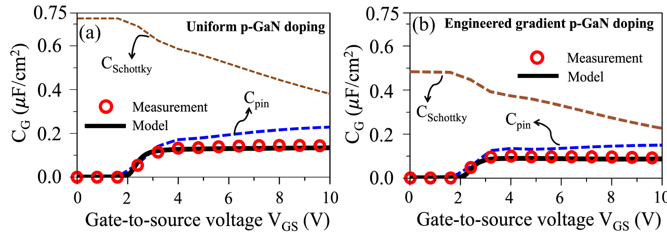

Fig. 7. Comparative analysis of characteristics between capacitance–voltage (C–V) measurements and a simplified model for (a) uniform p-GaN doping and (b) engineered gradient p-GaN doping. The inclusion of a low-doped p-GaN layer results in a notable reduction in the Schottky capacitance (C_{Schottky}).

$\Delta\psi_{\text{ch}}$)). Meanwhile, the capacitance of the Schottky diode is described as follows:

$$C_{\text{Schottky}} = \sqrt{\frac{q\varepsilon_{\text{GaN}}N_A}{2(V_{bi})}} \times \frac{1}{\left(1+\frac{\Delta V_j}{V_{bi}}\right)^m}. \tag{13}$$

Fig. 7 presents a comparative analysis between a theoretical model and experimental measurements for two distinct scenarios: 1) uniform p-GaN doping and 2) engineered gradient p-GaN doping. The results indicate an agreement between the model and the experimental data. The parameter represented by the symbol C_d, as specified in (10), is determined to be 0.31 μF/cm^2. For uniform p-GaN doping, the extracted 2-D Dos is 4.4×10^{13} cm^{-2}V^{-1}, whereas for engineered gradient p-GaN doping, it is 3.2×10^{13} cm^{-2}V^{-1}, and the extracted c is around 0.25, which is close to typical values reported [22]. The intentional modification of the p-GaN doping profile in a gradient manner results in an increased depletion depth. This deliberate alteration subsequently reduces the Schottky capacitance, thereby leading to a notable decrease in the gate capacitance.

B. Impact of Doping Profile Engineering on Gate Forward Breakdown Voltage: Model and Verification

Obviously, gate forward breakdown voltage occurs at high V_{GS} values. Using the engineered gradient p-GaN doping results in an increase of this gate breakdown voltage [Fig. 6(a)]. In p-GaN gate HEMTs, this forward gate breakdown is attributed to impact ionization. It is imperative to comprehend that, as depicted in Fig. 6(a), the adoption of engineered gradient p-GaN doping results in a reduction of the maximum electric field at the Schottky junction. Therefore, electrons must attain more energy in order to scatter and form pairs of electrons and holes, necessitating a higher V_{GS} to achieve this. As a result, this reduction in electric field contributes to a decrease in forward bias gate leakage current and an enhancement in breakdown voltage [23], [25].

A possible assumption is that the breakdown may occur in an effective depletion region in the p-GaN layer, which is referred to as the effective depletion depth (W_{eff}). This is important, since it is in this region that the electric field is constant at its maximum value. When a positive voltage is applied to the gate, the Schottky diode is effectively reverse biased. This Schottky diode plays a critical role in preventing gate leakage current. This diode acts as a barrier, causing most of the voltage applied to the gate to be dropped on ΔV_j linearly (at higher gate biases), as shown in Fig. 3. As a result of this process, eventually gate forward breakdown will occur earlier in uniformly doped p-GaN due to higher Mg concentrations, which creates a stronger electric field at the junction.

TABLE II
COMPARISON BETWEEN EXTRACTED BREAKDOWN VOLTAGE: MODEL VERSUS MEASUREMENT

V_{BR}	**Uniform doping**	**Engineered doping**
Measurement	10.9 V	14.8 V
Model	11 V	14.7 V

The ionization coefficient is governed by the Okuto–Crowell model [26]

$$\alpha = A^* \times E \times \exp\left(-\frac{B^*}{E}\right) \tag{14}$$

where A^* and B^* are empirical coefficients, and the extracted values are 0.21 V^{-1} and 7.5×10^6 $V \times \text{cm}^{-1}$, respectively.

Our assumption here is that electric field is constant at its maximum value over an effective junction width W_{eff}

$$1 - \frac{1}{M} = \int_0^{W_d} \alpha dx = \alpha_{\max} W_{\text{eff}} \tag{15}$$

where M represents the multiplication factor ($M = (1/1 - ((V/V_{BR}))^{m^*}) = (1/1 - \alpha_{\max} W_{\text{eff}})$), with m^* ranging between 2 and 6; it is notable that breakdown happens when the value of $((\alpha_{\max} W_{\text{eff}})^{m^*})^{1/2}$ equals 1.

By computing the 1-D electric field (E) in the p-GaN layer and substituting the result into (15), we obtain W_{eff}

$$W_{\text{eff}} = \exp\left(\frac{B^*}{E_{\max}}\right) \int_0^{Wd} \left(1 - \frac{x}{W_d}\right) \times \exp\left(\frac{-B^*}{E_{\max}\left(1 - \frac{x}{W_d}\right)}\right) dx. \tag{16}$$

Equation (16) is not efficient for compact modeling and may not have a closed-form solution. According to [27], the effective depletion depth ratio can be conveniently expressed over a relatively wide voltage range as follows:

$$\frac{W_{\text{eff}}}{W_d} = C \times \left(\frac{B^*}{E_{\max}}\right)^{-p} \tag{17}$$

where C and p represent the fitted parameters, extracted as 0.6 and 0.41, respectively, and the maximum electric field at the Schottky contact is calculated as follows:

$$E_{\max} = \frac{2(V_{bi} + \Delta V_j)}{W_d}. \tag{18}$$

Table II presents a comparison between the extracted breakdown voltage obtained via modeling and measurement, revealing a remarkably close correspondence between the model and the measurement.

This article has been accepted for inclusion in a future issue of this journal. Content is final as presented, with the exception of pagination.

V. Conclusion

An integrated continuous model is presented in this article, which encompasses the 2DEG charge, as well as the junction and barrier voltages, gate capacitance, and breakdown voltage. The 2DEG charge saturation due to the AlGaN barrier height saturation makes this model applicable to a broad range of gate-to-source voltages up to forward gate bias breakdown. The proposed model's accuracy is substantiated by rigorous validation against TCAD numerical simulations. Moreover, we examined the influence of employing engineered gradient p-GaN doping on several parameters, such as gate capacitance and forward gate breakdown. Subsequently, we formulated models for these parameters and validated their accuracy against measured data. By utilizing the present model, significant progress is being made toward facilitating circuit design and simulation.

References

[1] K. J. Chen et al., "GaN-on-Si power technology: Devices and applications," *IEEE Trans. Electron Devices*, vol. 64, no. 3, pp. 779–795, Mar. 2017.

[2] S.-W. Tang et al., "Using gate leakage conduction to understand positive gate bias induced threshold voltage shift in p-GaN gate HEMTs," *IEEE Trans. Electron Devices*, vol. 70, no. 2, pp. 449–453, Feb. 2023.

[3] A. Stockman, E. Canato, M. Meneghini, G. Meneghesso, P. Moens, and B. Bakeroot, "Schottky gate induced threshold voltage instabilities in p-GaN gate AlGaN/GaN HEMTs," *IEEE Trans. Device Mater. Rel.*, vol. 21, no. 2, pp. 169–175, Jun. 2021.

[4] S. Ghosh, S. A. Ahsan, A. Dasgupta, S. Khandelwal, and Y. S. Chauhan, "GaN HEMT modeling for power and RF applications using ASM-HEMT," in *Proc. 3rd Int. Conf. Emerg. Electron. (ICEE)*, Dec. 2016, pp. 1–4.

[5] F. Jazaeri and J.-M. Sallese, "Charge-based EPFL HEMT model," *IEEE Trans. Electron Devices*, vol. 66, no. 3, pp. 1218–1229, Mar. 2019.

[6] M. Allaei, M. Shalchian, and F. Jazaeri, "Modeling of short-channel effects in GaN HEMTs," *IEEE Trans. Electron Devices*, vol. 67, no. 8, pp. 3088–3094, Aug. 2020.

[7] U. Radhakrishna, P. Choi, and D. A. Antoniadis, "Facilitation of GaN-based RF- and HV-circuit designs using MVS-GaN HEMT compact model," *IEEE Trans. Electron Devices*, vol. 66, no. 1, pp. 95–105, Jan. 2019.

[8] A. Sarkar and Y. M. Haddara, "Modeling of forward gate leakage current for normally off pGaN/AlGaN/GaN HEMTs," *Solid-State Electron.*, vol. 196, Oct. 2022, Art. no. 108420.

[9] N. Xu et al., "Gate leakage mechanisms in normally off p-GaN/AlGaN/GaN high electron mobility transistors," *Appl. Phys. Lett.*, vol. 113, no. 15, Oct. 2018, Art. no. 153501.

[10] A. Abdulsalam and G. Dutta, "On the threshold voltage of normally-OFF AlGaN/GaN heterostructure field effect transistors (HFETs) with p-(Al)GaN gate," *Semicond. Sci. Technol.*, vol. 35, no. 1, Jan. 2020, Art. no. 015020.

[11] N. Modolo, S.-W. Tang, H.-J. Jiang, C. De Santi, M. Meneghini, and T.-L. Wu, "A novel physics-based approach to analyze and model E-mode p-GaN power HEMTs," *IEEE Trans. Electron Devices*, vol. 68, no. 4, pp. 1489–1494, Apr. 2021.

[12] B. Bakeroot, S. Stoffels, N. Posthuma, D. Wellekens, and S. Decoutere, "Trading off between threshold voltage and subthreshold slope in AlGaN/GaN HEMTs with a p-GaN gate," in *Proc. 31st Int. Symp. Power Semicond. Devices ICs (ISPSD)*, May 2019, pp. 419–422, doi: 10.1109/ISPSD.2019.8757629.

[13] T.-L. Wu et al., "Analysis of the gate capacitance–voltage characteristics in p-GaN/AlGaN/GaN heterostructures," *IEEE Electron Device Lett.*, vol. 38, no. 12, pp. 1696–1699, Dec. 2017.

[14] B. Bakeroot, A. Stockman, N. Posthuma, S. Stoffels, and S. Decoutere, "Analytical model for the threshold voltage of *p*-(Al)GaN high-electron-mobility transistors," *IEEE Trans. Electron Devices*, vol. 65, no. 1, pp. 79–86, Jan. 2018.

[15] N. E. Posthuma et al., "Impact of Mg out-diffusion and activation on the p-GaN gate HEMT device performance," in *Proc. 28th Int. Symp. Power Semicond. Devices ICs (ISPSD)*, Jun. 2016, pp. 95–98.

[16] I. Vurgaftman and J. R. Meyer, "Nitride semiconductor devices," in *Nitride Semiconductor Devices: Principles and Simulation*. Hoboken, NJ, USA: Wiley, 2007, ch. 2.

[17] M. E. Levinshtein, S. L. Rumyantsev, and M. S. Shur, *Properties of Advanced Semiconductor Materials: GaN, AIN, InN, BN, SiC, SiGe*. Hoboken, NJ, USA: Wiley, 2001.

[18] J. Piprek, *Nitride Semiconductor Devices: Principles and Simulation*. Hoboken, NJ, USA: Wiley, 2007.

[19] N. Karumuri, S. Turuvekere, N. DasGupta, and A. DasGupta, "A continuous analytical model for 2-DEG charge density in AlGaN/GaN HEMTs valid for all bias voltages," *IEEE Trans. Electron Devices*, vol. 61, no. 7, pp. 2343–2349, Jul. 2014.

[20] W. Deng, J. Huang, X. Ma, and J. J. Liou, "An explicit surface potential calculation and compact current model for AlGaN/GaN HEMTs," *IEEE Electron Device Lett.*, vol. 36, no. 2, pp. 108–110, Feb. 2015.

[21] J. Blakemore, "Approximations for Fermi-Dirac integrals, especially the function F_{12} (η) used to describe electron density in a semiconductor," *Solid-State Electron.*, vol. 25, no. 11, pp. 1067–1076, 1982.

[22] N. S. Swamy and A. K. Dutta, "Analytical models for the 2DEG density, AlGaN layer carrier density, and drain current for AlGaN/GaN HEMTs," *IEEE Trans. Electron Devices*, vol. 65, no. 3, pp. 936–944, Mar. 2018.

[23] M. Borga, N. Posthuma, A. Vohra, B. Bakeroot, and S. Decoutere, "Enhancing the forward gate bias robustness in p-GaN gate high-electron-mobility transistors through doping profile engineering," *Phys. Status Solidi (A)*, vol. 1, Apr. 2024, Art. no. 2400043.

[24] M. Alaei, M. Borga, E. Fabris, S. Decoutere, J. Lauwaert, and B. Bakeroot, "Modeling gate leakage current for p-GaN gate HEMTs with engineered doping profile," *IEEE Trans. Electron Devices*, vol. 71, no. 8, pp. 4563–4569, Aug. 2024.

[25] G. Zhou et al., "P-GaN gate HEMTs with 10.6 V maximum gate drive voltages by Mg doping engineering," *IEEE Trans. Electron Devices*, vol. 69, no. 5, pp. 2282–2286, May 2022.

[26] Y. Okuto and C. Crowell, "Threshold energy effect on avalanche breakdown voltage in semiconductor junctions," *Solid-State Electron.*, vol. 18, no. 2, pp. 161–168, 1975.

[27] P. Mars, "Temperature dependence of avalanche breakdown voltage temperature dependence of avalanche breakdown voltage in p–n junctions," *Int. J. Electron.*, vol. 32, no. 1, pp. 23–37, Jan. 1972.